PLOS | ONE

RESEARCH ARTICLE

Mechanistic and Kinetic Analysis of Na_2SO_4-Modified Laterite Decomposition by Thermogravimetry Coupled with Mass Spectrometry

Song Yang[1], Wenguang Du[1], Pengzheng Shi[1], Ju Shangguan[1]*, Shoujun Liu[2], Changhai Zhou[2], Peng Chen[2], Qian Zhang[1], Huiling Fan[1]

1 Key Laboratory for Coal Science and Technology of Ministry of Education and Shanxi Province, Institute for Chemical Engineering of Coal, Taiyuan University of Technology, Taiyuan 030024, China, **2** College of Chemistry and Chemical Engineering, Taiyuan University of Technology, Taiyuan 030024, China

* shanggj62@163.com

OPEN ACCESS

Citation: Yang S, Du W, Shi P, Shangguan J, Liu S, Zhou C, et al. (2016) Mechanistic and Kinetic Analysis of Na_2SO_4-Modified Laterite Decomposition by Thermogravimetry Coupled with Mass Spectrometry. PLoS ONE 11(6): e0157369. doi:10.1371/journal.pone.0157369

Editor: G Y, Southwest University, CHINA

Received: December 19, 2015

Accepted: May 28, 2016

Published: June 22, 2016

Data Availability Statement: All relevant data are within the paper.

Funding: This work was financially supported by the National Natural Science Foundation of China (No. 21276172) and sponsored by the Taiyuan Green Coal-based Clean Fuel Co., Ltd. (China). The funders had no role in study design, data collection and analysis, decision to publish, or preparation of the manuscript.

Competing Interests: The authors have declared that no competing interests exist.

Abstract

Nickel laterites cannot be effectively used in physical methods because of their poor crystallinity and fine grain size. Na_2SO_4 is the most efficient additive for grade enrichment and Ni recovery. However, how Na_2SO_4 affects the selective reduction of laterite ores has not been clearly investigated. This study investigated the decomposition of laterite with and without the addition of Na_2SO_4 in an argon atmosphere using thermogravimetry coupled with mass spectrometry (TG-MS). Approximately 25 mg of samples with 20 wt% Na_2SO_4 was pyrolyzed under a 100 ml/min Ar flow at a heating rate of 10°C/min from room temperature to 1300°C. The kinetic study was based on derivative thermogravimetric (DTG) curves. The evolution of the pyrolysis gas composition was detected by mass spectrometry, and the decomposition products were analyzed by X-ray diffraction (XRD). The decomposition behavior of laterite with the addition of Na_2SO_4 was similar to that of pure laterite below 800°C during the first three stages. However, in the fourth stage, the dolomite decomposed at 897°C, which is approximately 200°C lower than the decomposition of pure laterite. In the last stage, the laterite decomposed and emitted SO_2 in the presence of Na_2SO_4 with an activation energy of 91.37 kJ/mol. The decomposition of laterite with and without the addition of Na_2SO_4 can be described by one first-order reaction. Moreover, the use of Na_2SO_4 as the modification agent can reduce the activation energy of laterite decomposition; thus, the reaction rate can be accelerated, and the reaction temperature can be markedly reduced.

Introduction

Nickel has good plasticity, corrosion resistance and magnetic properties and is widely used in the iron and steel, nickel-based alloy electroplating, and the battery industries. These uses have led to a dramatic increase in the production of nickel in recent years [1]. Nickel can be obtained

from nickel sulfide ores and nickel laterite ores. Although nickel sulfide ores can be treated to make them easier to process to obtain high grade nickel and improve recovery, they are becoming increasingly rare. Therefore, nickel laterite, which composes more than 70% of nickel resources and is easy to mine and transport, has attracted large amounts of attention in recent years and will be the main source of nickel in the future [2].

Nickel laterite ores can be divided into two different types based on their chemical and physical characteristics: saprolitic and limonitic ores [3]. Saprolitic ores contain a heterogeneous distribution of quartz, talc, serpentine, olivine, garnierite and high-grade nickel. Limonitic ores are buried near the ground surface and contain goethite, gibbsite, and chromite [4,5]. However, these nickel laterites cannot be effectively used in physical methods because of their poor crystallinity and fine grain size. Moreover, nickel cannot be identified in laterites by normal X-ray diffraction (XRD) detectors because of their low Ni concentrations and variable distributions. Goethite and silicate minerals (lizardite and olivine) are the Ni host phases [6]. Therefore, effectively upgrading these ores by physical treatment processes can be challenging. To solve this problem, pyrometallurgical production methods have been applied to extract nickel from laterite ores, which can obtain high nickel recoveries [7]. However, because of their high energy consumption and the low accumulation rate of Ni, the use of these methods is limited by low-grade laterite ores and extremely high operating temperatures [8]. Therefore, pre-reduction followed by magnetic separation has been proposed as an easy, low-energy-consumption and environmentally friendly process [9,10]. Laterite contains large amounts of water, which includes water that is adsorbed on the crystals and water in the mineral structure [1,7]. Water makes up 35% of the total quantity of the laterite; thus, laterite must be dried before the pre-reduction process. Moreover, the complex mineral composition of laterite will strongly affect the reduction roasting process. Therefore, studying the decomposition of laterite is important for the pre-reduction of laterite.

Recently, several researchers have focused on the reductive roasting of laterite ore with different reductants, such as carbon, CO or H_2, followed by magnetic separation [9,10]. Reductive roasting of laterite can provide high nickel recovery, but the grade of the nickel remains low. Because nickel is hosted in goethite and silicate minerals, something must be added to break the bonds of the silicate and nickel; the nickel can then be easily reduced by a reductant. Therefore, additives such as Na_2CO_3, S, NaCl and Na_2SO_4 are used to enhance the enrichment ratio of Ni and reduce the reaction temperature [11,12]. Na_2SO_4 is the most efficient additive in terms of both grade enrichment and the recovery of Ni. The addition of 10–20 wt% Na_2SO_4 and 2% wt% coal, which was reduced at 1100–1200°C, resulted in a Ni content of 9.87% and a nickel recovery of 90.90% [11,12]. The Na_2SO_4 has two main effects: forming low-melting-point FeS to aggregate the ferronickel particles and suppressing the reduction of the ferrous minerals [13]. However, exactly how Na_2SO_4 reacts with laterite and when the reaction occurs has not been clearly investigated. Considering the potential application of Na_2SO_4 as a modification agent, the optimal operational conditions of the system should be determined. Based on the discussion presented above, this study investigated the decomposition characteristics of laterite with and without the addition of Na_2SO_4 using thermogravimetry coupled with mass spectrometry (TG-MS) to explore the effect of Na_2SO_4 on laterite decomposition. To further explore the reduction-promoting mechanisms of Na_2SO_4 on laterite ores, we also performed reduction roasting experiments of laterite ores with and without Na_2SO_4 at different roasting temperature points. The results of this study may provide a reference for the application of additives in related industries.

Materials and Methods

Materials

The feedstock material that was used in this study was a low-grade laterite ore from Indonesia. The as-received sample was ground to a particle size of less than 0.83 mm. Reagent-grade sodium sulfate was selected as the modification reagent.

An inductively coupled plasma atomic emission spectrometer (ICP-AES-9000(N+M)), which was a commercial product of Thermo Jarrell-Ash Corp., USA, was used to determine the chemical composition of the materials. A chemical phase analysis was performed to identify the distribution of nickel in the laterite; the results are listed in Table 1.

Table 1 shows the main chemicals and the nickel distribution of the studied laterite, which contained 1.41 wt% Ni, 24.14 wt% Fe, 14.58 wt% MgO, 29.36 wt% SiO_2 and 3.15 wt% Al_2O_3 and thus was a typical saprolite laterite [14]. The nickel was mainly hosted in silicate minerals (84.40%).

Methods

Samples

The laterite ore was mixed with sodium sulfate by mechanical stirring. The content of the sodium sulfate was 20 wt%, and the corresponding samples were denoted by Na_2SO_4/laterite blend ores. Laterite ore without Na_2SO_4 was used as the control.

Laterite decomposition

The decomposition of the laterite was carried out using a Setaram SETSYS TGA coupled with a Hiden HPR20 QIC R&D mass spectrometer. Approximately 25 mg of the sample was pyrolyzed under a 100 ml/min Ar flow at a heating rate of 10°C/min from room temperature to 1300°C. The mass loss (TG) and the derivative thermogravimetric (DTG) curves with the temperature were obtained from the results of the experiment [15]. The kinetic study was based on the derivative DTG curves. The evolved gaseous compounds that were generated during the decomposition of the laterite were detected by MS. The different crystalline phases of the ores were determined by XRD using Cu-Kα radiation with a scanning rate of 3°/min from 5°–85° [15].

To ensure the uniformity of the sample and considering the small amount needed for the TG test, three sets of duplicate experiments were performed.

Decomposition of the Na_2SO_4/laterite blends

The samples of the Na_2SO_4/laterite blends were subjected to pyrolysis following a process similar to that described in the preceding subsection. MS and XRD were performed.

Three sets of duplicate experiments were performed for the TG test.

Table 1. The main chemicals and nickel distribution of the studied laterite (wt%).

	Nickel distribution state of the studied laterite ore								
Ni_{total}	Adsorption			Sulfides		Oxides		Silicates	
1.41	0.03			0.07		0.12		1.19	
Fe_{total}	Cr_2O_3	Al_2O_3	CaO	MgO	SiO_2	P_2O_5	MnO_2	Co	LOI[a]
24.14	1.08	3.15	1.46	14.58	29.36	0.018	1.46	0.065	12.95

[a]LOI: Loss on ignition.

doi:10.1371/journal.pone.0157369.t001

Kinetic analysis

The kinetic parameters were determined by the integral method, which assumed that the decomposition of laterite with and without the addition of Na_2SO_4 occurred in multiple stages and is a first-order reaction for each stage [16–18]. The following results indicate that this assumption is reasonable. The rate reactions of the solid-state can be then expressed using differential kinetic equations [19–20]. The decomposition reaction of laterite with and without the addition of Na_2SO_4 was obtained from the literature [18] and is expressed by the following formula:

$$\frac{d\alpha}{dt} = \mathrm{k(t)} \cdot f(\alpha) \tag{1}$$

where α is the decomposition conversion, t is time, k(t) is the temperature-dependent rate constant, and $f(\alpha)$ is a function that represents the reaction model.

The decomposition conversion, α, can be expressed by [18]

$$\alpha = \frac{W_0 - W_t}{W_0 - W_f} \tag{2}$$

where W_0 is the original weight of the test sample, W_t is the weight at time t, and W_f is the final weight at the end of the decomposition.

Generally, k(t) is written as an Arrhenius relation [21]:

$$\mathrm{k(t)} = A\exp\left(-\frac{E}{RT}\right)f(\alpha) \tag{3}$$

where E is the activation energy, A is the pre-exponential factor, and T is the temperature.

Because $\Theta = dT/dt$, which is a constant heating rate, we can rearrange and integrate Eq (3); the integration can then be expressed as follows [22]:

$$\ln\left[\frac{-\ln(1-\alpha)}{T^2}\right] = ln\left[\frac{AR}{\Theta E}\left(1 - \frac{2RT}{E}\right)\right] - \frac{E}{RT} \tag{4}$$

Because Θ is a constant (10°C/min) during decomposition and the temperature range of laterite decomposition is much larger than $2RT$ for most values of E, the expression $2RT/E$ is nearly equal to 0 [16]. Therefore, Eq (4) can be rearranged as follows [19]:

$$\ln\left[\frac{-\ln(1-\alpha)}{T^2}\right] = ln\left(\frac{AR}{10E}\right) - \frac{E}{RT} \tag{5}$$

The straight line that can be obtained from the left side of Eq (5) is plotted versus 1/T because the process can be assumed to be a first-order reaction.

The evolutions of the weight and weight loss rate with increasing temperature were obtained for the decomposition. The weight loss rate was calculated by the following expression [23]:

$$\frac{dW}{dt} = -\frac{1}{W_0}\left(\frac{dWt}{dt}\right) \tag{6}$$

where W_0 is the original weight of the test sample, and W_t is the weight at time t.

Reduction experiments

Laterite with 20% Na_2SO_4 with a combined mass of 100 g was prepared for the reduction process, which was performed in a stirred fixed-bed reactor [9]. After the samples were heated to

the determined temperature (700, 800, or 900°C) under a nitrogen flow rate of 0.7 L/min, a reaction was achieved by mixing gas (70% H_2 and 30% N_2) at 2.7 L/min for 120 min. The N_2 was used as a protective gas as the reduction process completed until the samples cooled to room temperature.

The reduced samples were ground to 90 wt% passing 0.043 mm using a rod mill. Then, approximately 5 g of each ground sample was separated in an XCGS-73 Davies magnetic tube with a magnetic field intensity of 0.1 T [7]. The final magnetic product consisted of FeNi concentrates. The content of Fe and Ni in each sample was determined by chemical analysis. The recovery rate of Fe and Ni was calculated as described in the literature [9].

The reduced products were analyzed using scanning electron microscopy (SEM; Carl Zeiss EVO18, Germany) according to the literature [11].

Results and Discussion

Decomposition of laterite with and without the addition of Na_2SO_4

Figs 1 and 2 show the TG and DTG curves of the decomposition of the laterite nickel ore and the Na_2SO_4/laterite blends, respectively. The weights of both samples decreased with increasing temperature.

In Fig 1, four obvious stages of mass loss were identified. The first stage reaction occurred between 34°C and 100°C and included the evaporation of the free water in the laterite. The

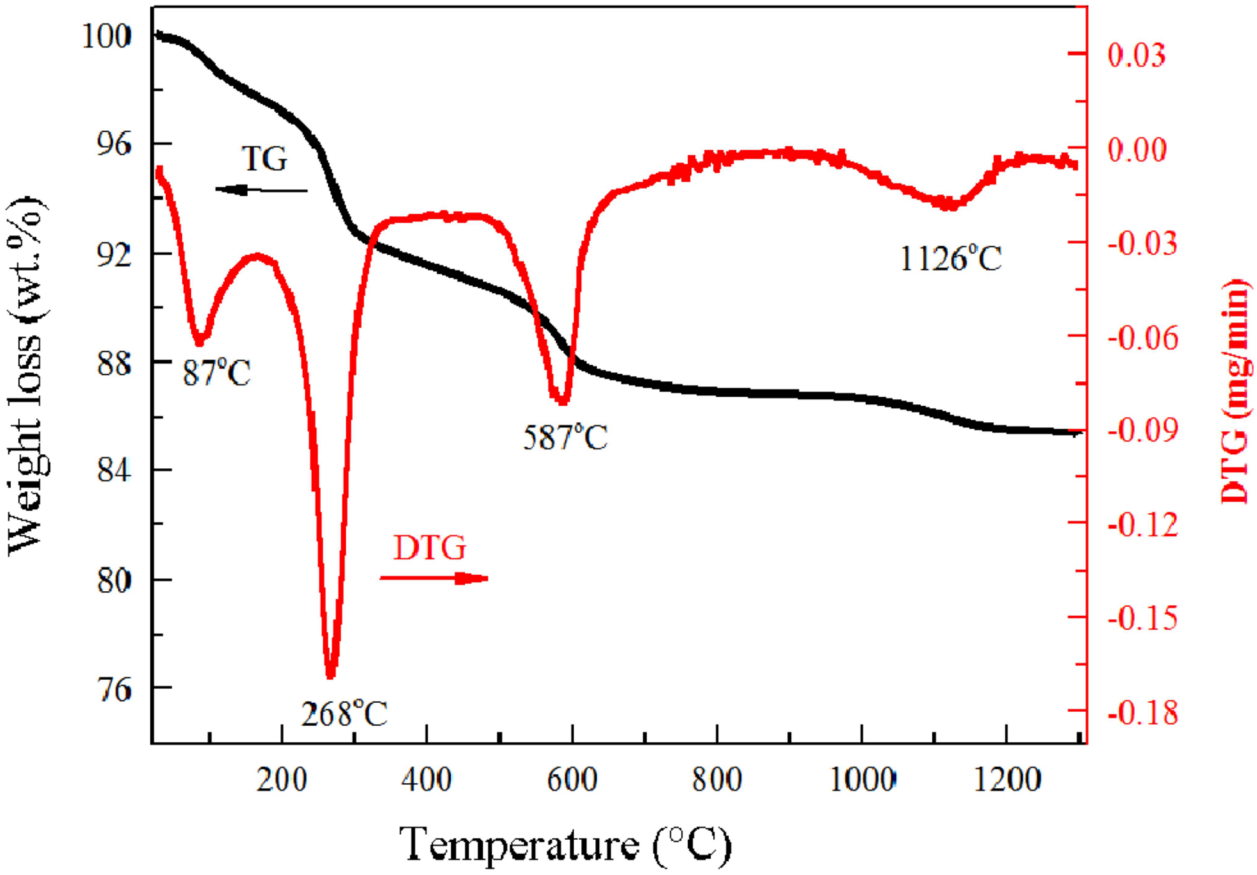

Fig 1. Differential thermal analysis–TGA curves for laterite.

doi:10.1371/journal.pone.0157369.g001

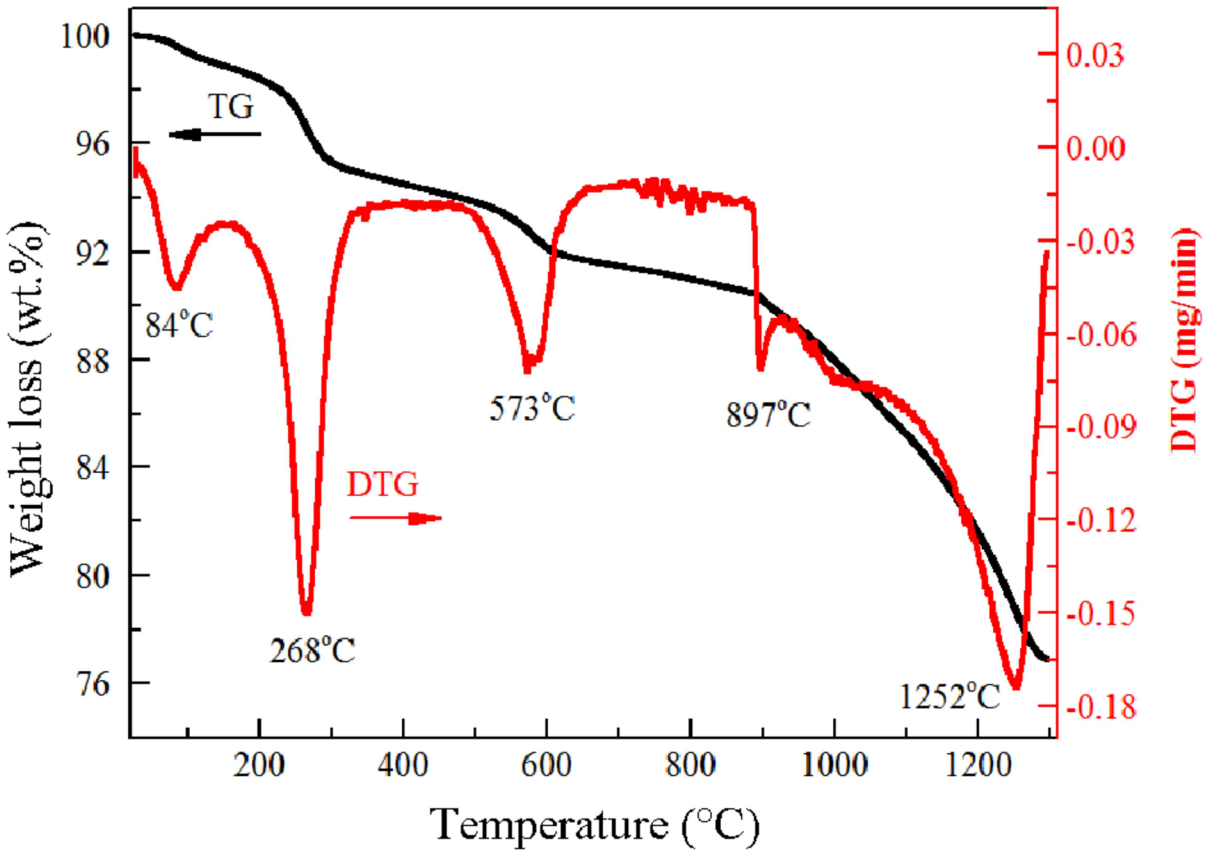

Fig 2. Differential thermal analysis–TGA curves for the Na_2SO_4/laterite blends.

doi:10.1371/journal.pone.0157369.g002

second stage was between 238°C and 278°C and was caused by the transformation of goethite ores to iron oxide. The third stage involved the dehydroxylation of kaolinite and serpentine and occurred between 554°C and 602°C. The last stage occurred between 1100°C and 1145°C and involved only 3% of the total mass loss.

In Fig 2, five stages of mass loss were identified. Before reaching 863°C, the weight loss curves of the Na_2SO_4/laterite blends displayed almost the same trend as those of the laterite, which indicates that they had the same decomposition behavior. At temperatures of 987–1300°C, the TG curves of the Na_2SO_4/laterite blends decreased sharply compared to those of laterite, which is attributed to the decomposition of Na_2SO_4; Na_2SO_4 thus reacted with laterite in this temperature range.

Tables 2 and 3 show the parameters that were obtained from the decomposition experiments, including the initial decomposition temperature (T_I), the final decomposition temperature (T_F), the corresponding peak temperatures (T_P), and the maximum weight loss rates

Table 2. Characteristic parameters of laterite decomposition (wt%).

Stage	Decomposition range (°C)		$(dW_i/dt)_{max}$ (min^{-1})	Peak temperature (°C)
	T_I	T_F		T_P
a	238	278	-0.1684	268
b	554	602	-0.08106	587
c	1100	1145	-0.01893	1126

doi:10.1371/journal.pone.0157369.t002

Table 3. Characteristic parameters of Na_2SO_4/laterite blend decomposition (wt%).

Stage	Decomposition range (°C)		$(dW_i/dt)_{max}$ (min^{-1})	Peak temperature (°C)
	T_I	T_F		T_P
a	238	278	-0.1177	268
b	554	602	-0.0562	573
c	892	914	-0.0556	897
d	1241	1286	-0.1368	1252

doi:10.1371/journal.pone.0157369.t003

$(dW_i/dt)_{max}$. From room temperature to 100°C, free water evaporated from the samples, which made the determination of T_I difficult [24,25]. Regular decomposition data cannot be obtained until 238°C; therefore, the initial temperature of decomposition T_I is defined as 238°C.

At 600°C, the weight loss without Na_2SO_4 is 11.18 wt%, but with Na_2SO_4, it is 8.86 wt%. As Na_2SO_4 cannot be decomposed at 600°C and as the initial the initial Na_2SO_4 content of the Na_2SO_4/laterite blends was 20 wt% Na_2SO_4, the weight loss of the Na_2SO_4/laterite blends was due to the decomposition of laterite alone. Then, based on the weight of the 20 wt% Na_2SO_4, we can deduce that the weight loss is 11.08 wt%, which is similar to the weight loss without Na_2SO_4.

When the decomposition of the laterite nickel ore is complete at 1300°C, the volatile content is approximately 14.63 wt%. The decomposition of the Na_2SO_4/laterite blends produces approximately 23.12 wt% of volatiles under the same experimental conditions.

From room temperature to 890°C, the laterite and the Na_2SO_4/laterite blends have similar corresponding peak temperatures in their DTG curves. At temperatures higher than 897°C, the decomposition of laterite has only one peak temperature in its DTG curve at 1126°C, but the Na_2SO_4/laterite blends have two peak temperatures at 897°C and 1252°C.

Kinetic characteristics

The values of E and A (pre-exponential factor) can be determined by Eq (3) and are shown in Tables 4 and 5, respectively.

Figs 3 and 4 show plots of $ln(-ln(1-\alpha)/T^2)$ versus $1/T$, respectively. The plots for laterite are similar to those for the Na_2SO_4/laterite blends at temperatures between room temperature and 890°C. However, above 897°C, laterite behaves differently from the Na_2SO_4/laterite blends.

The kinetic parameters are calculated from the characteristic peaks, which were selected from Figs 1 and 2. Thus, these plots can be represented by the main decomposition region. From Figs 3 and 4, the plots of $ln(-ln(1-\alpha)/T^2)$ versus $1/T$, 7 straight lines can be obtained, which indicated that the laterite decomposition and Na_2SO_4/laterite blend decomposition can be classified as a first order reaction. Therefore, the entire decomposition process can be described by one first-order reaction, which is consistent with the results from the literature [16–18].

The relative activation energies of the decomposition of laterite closely resemble those of the Na_2SO_4/laterite blends, which indicates that Na_2SO_4 did not change the decomposition of

Table 4. Kinetic parameters for laterite decomposition.

Stage	Temp (°C)	Conversion range (%)	E (kJ/mol)	A (min^{-1})	R^2
a	238–278	25.88–42.43	87.13	2.83×10^5	0.9947
b	554–602	70.44–81.18	123.63	9.75×10^4	0.9927
c	1100–1145	94.77–97.21	145.66	2.82×10^5	0.9999

doi:10.1371/journal.pone.0157369.t004

Table 5. Kinetic parameters for the decomposition of Na_2SO_4/laterite blends.

Stage	Temp (°C)	Conversion range (%)	E (kJ/mol)	A (min^{-1})	R^2
a	238–278	9.88–17.50	66.35	2.77×10^5	0.9968
b	554–602	29.57–34.19	109.58	1.43×10^5	0.9939
c	892–914	41.50–43.68	108.50	2.58×10^5	0.9930
d	1241–1286	89.09–99.24	91.37	4.14×10^6	0.9832

doi:10.1371/journal.pone.0157369.t005

laterite between room temperature and 897°C. The melting point of Na_2SO_4 is 884°C [26], which is very close to 897°C. As the solid-state reaction requires more energy than the solid-liquid heterogeneous reactions [27], when the Na_2SO_4 begins to melt, it can accelerate the reaction of Na_2SO_4 with laterite. Therefore, the temperature of 897°C, which yields one of the fastest reaction rates, is very close to the melting point of Na_2SO_4.

However, above 897°C, the Na_2SO_4/laterite blends are different from laterite, which undergoes only one reaction with a relative activation energy of 145.66 kJ/mol. In the presence of Na_2SO_4, there are two reaction processes with relative activation energies of 108.50 and 91.37 kJ/mol.

Li et al. reported a lower melting point in the presence of Na_2SO_4, which could lead to the precipitation of larger particles [12]. Therefore, Na_2SO_4 significantly influences laterite decomposition through direct involvement and by changing the mechanism. Although adding Na_2SO_4 cannot change the reaction order, it can reduce the activation energy of laterite decomposition; thus, the reaction rate could be accelerated, and the reaction temperature could be markedly reduced.

Decomposition mechanism

Laterite decomposition mechanism. To identify the mechanism of laterite decomposition, the laterite ores were roasted under a 100 ml/min Ar flow for 4 h at temperatures of 87°C, 268°C, 587°C, and 1126°C.

The phase of the roasted ores can be elucidated from the XRD patterns (Fig 5), and the volatile component was analyzed by TG-MS. The variations in the H_2O content during the thermal decomposition of laterite with and without the addition of Na_2SO_4 are shown in Figs 6 and 7, respectively.

Figs 1, 5 and 6 show that the decomposition process of laterite can be divided into four stages. The first stage (34°C<T<100°C) included the evaporation of the free water in the laterite. In the second stage (238°C<T<278°C), the goethite phase disappears after being roasted

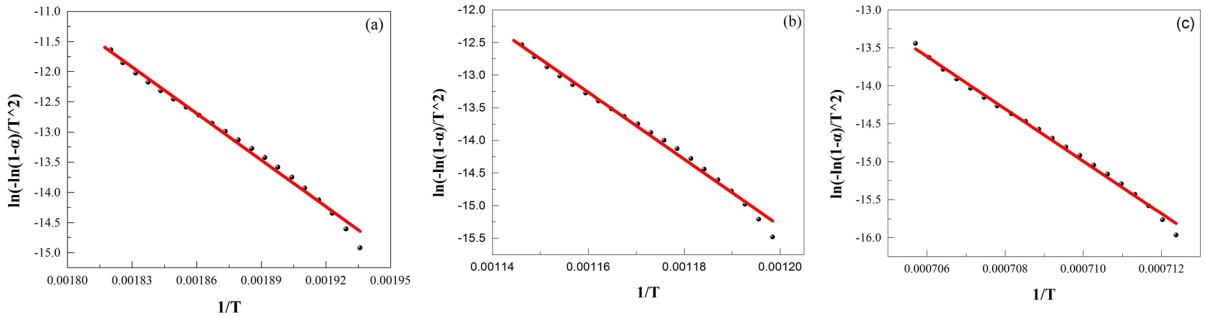

Fig 3. Plots of $ln(-ln(1-\alpha)/T^2)$ vs. $1/T$ for laterite decomposition recalculated by the multi-step integral method. (a), 238–278°C; (b), 554–602°C; (c), 1100–1145°C.

doi:10.1371/journal.pone.0157369.g003

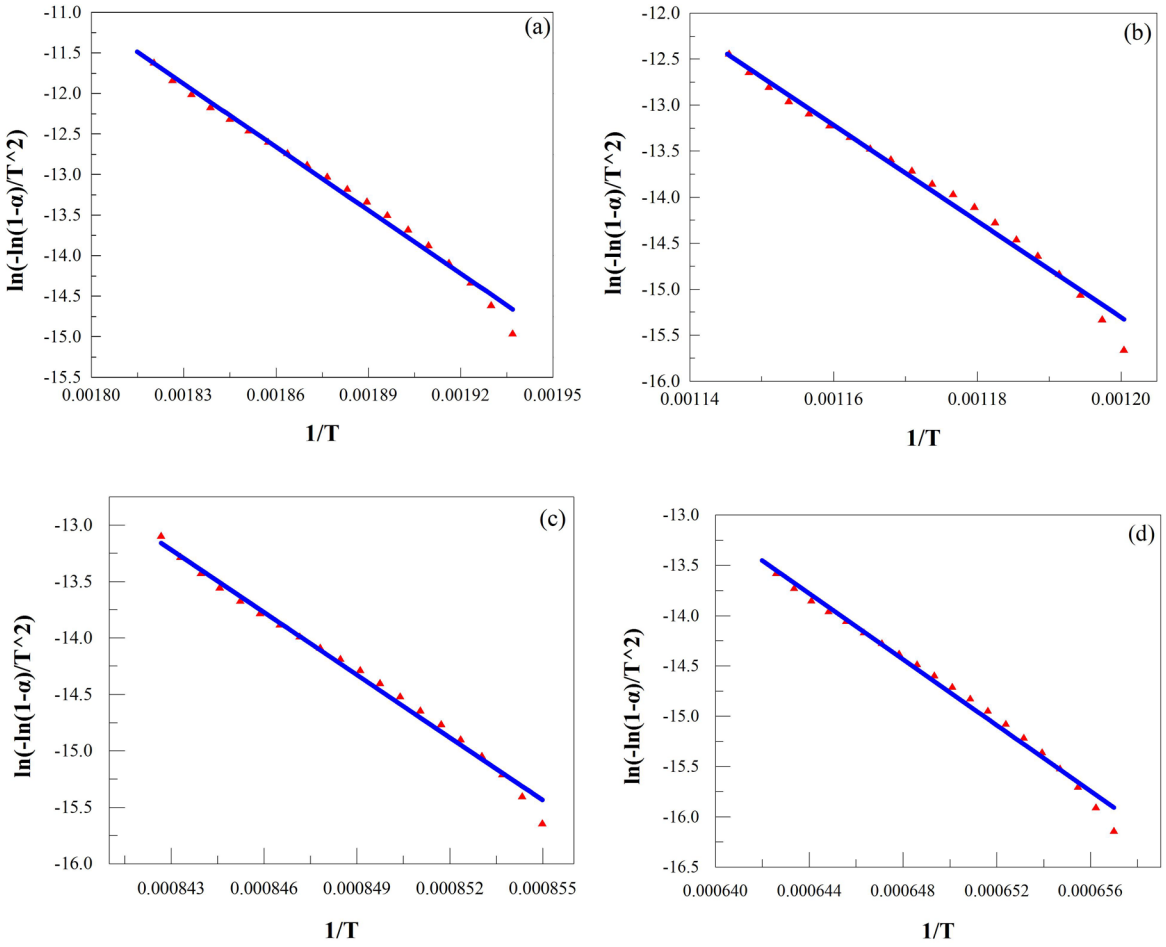

Fig 4. Plots of $ln(-ln(1-\alpha)/T^2)$ vs. $1/T$ for Na_2SO_4/laterite blend decomposition recalculated by the multi-step integral method. (a), 238–278°C; (b), 554–602°C; (c), 892–914°C; (d), 1241–1286°C.

doi:10.1371/journal.pone.0157369.g004

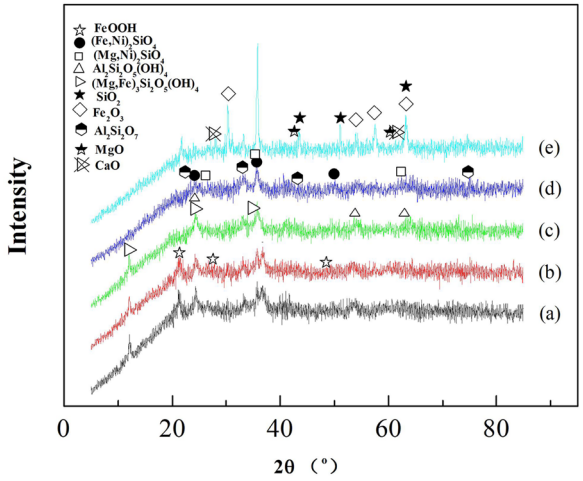

Fig 5. XRD patterns of laterite ores roasted under Ar at different temperatures. (a) raw ore, (b) 87°C, (c) 268°C, (d) 587°C, (e) 1126°C.

doi:10.1371/journal.pone.0157369.g005

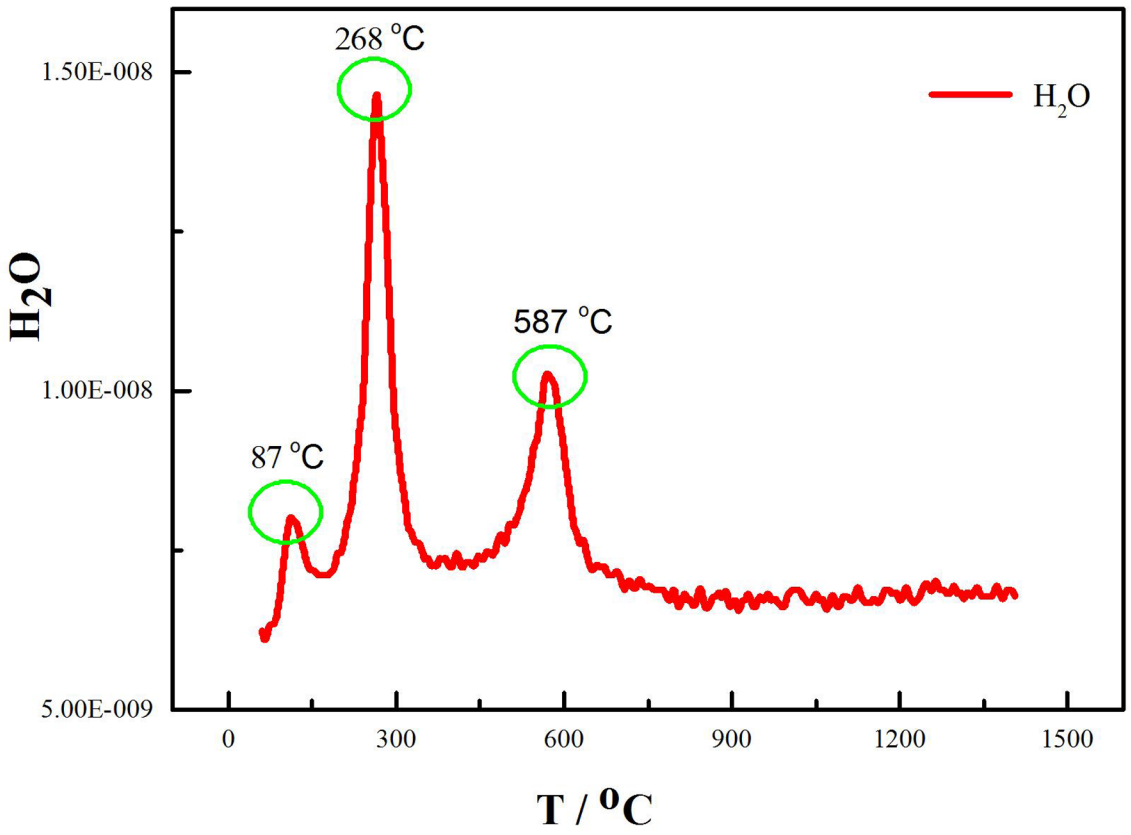

Fig 6. MS fragmentation intensities of H_2O during the thermal decomposition of the laterite.

doi:10.1371/journal.pone.0157369.g006

under Ar flow for 4 h (Fig 5B). Jang et al. investigated the transformation process of goethite ores to pure iron and found that water was released from the ores at low temperatures [28]. Our results show that water was the main volatile component in the second stage (Fig 6), which is consistent with results from the literature [28]. This process can be expressed by Eq (7):

$$2\alpha\text{–FeOOH(s)} = \alpha\text{–}Fe_2O_3(s) + H_2O(g) \quad (7)$$

As a result, new crystalline phases ($(Fe,Ni)_2SiO_4$, $(Mg,Ni)SiO_3$, $(Fe,Ni)_2SiO_4$, $(Fe,Ni)SiO_3$, SiO_2, $Al_2Si_2O_7$) formed (Fig 5C) during laterite decomposition at 587°C for 4 h, and the main volatile component was H_2O (Fig 6). The water was produced by the dehydroxylation of kaolinite and serpentine at temperatures between 554°C and 602°C [29]. The process can be expressed by the following formulas:

$$2(Mg, Fe, Ni)_3Si_2O_5(OH)_4 = (Mg, Ni)_3Si_2O_5(OH)_4 + (Fe, Ni)_3Si_2O_5(OH)_4 \quad (8)$$

$$2(Mg, Ni)_3Si_2O_5(OH)_4 = (Mg, Ni)_2SiO_4 + (Mg, Ni)SiO_3 + 2SiO_2 + H_2O \quad (9)$$

$$2(Fe, Ni)_3Si_2O_5(OH)_4 = (Fe, Ni)_2SiO_4 + (Fe, Ni)SiO_3 + 2SiO_2 + H_2O \quad (10)$$

$$Al_2Si_2O_5(OH)_4 = Al_2Si_2O_7 + 2H_2O \quad (11)$$

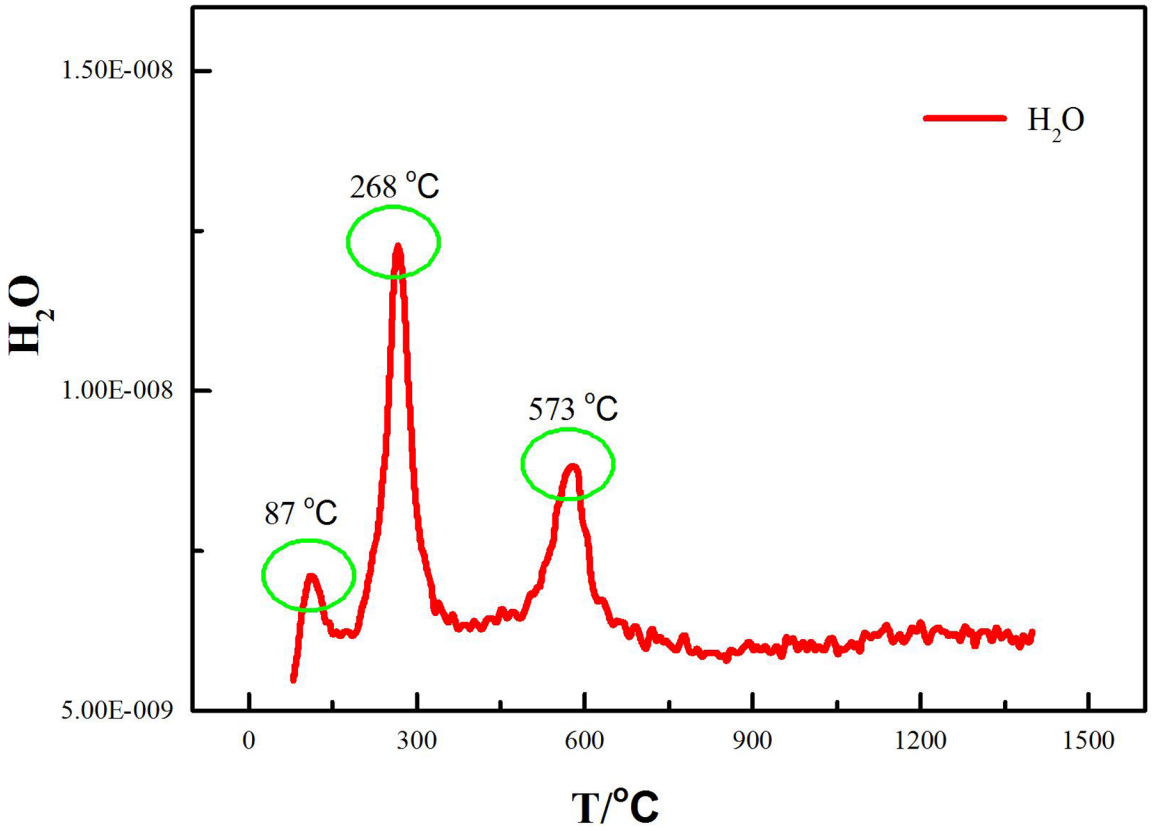

Fig 7. MS fragmentation intensities of H_2O during the thermal decomposition of the Na_2SO_4/laterite blends.

doi:10.1371/journal.pone.0157369.g007

The mechanism of laterite decomposition in the fourth stage (1100°C<T<1145°C) has not been determined in the literature. MS was used to identify the main volatile component in this temperature range, and the roasted sample, which was roasted under Ar flow for 4 h at 1126°C, was analyzed with XRD to identify the main component of the decomposition of the laterite. Fig 5D shows that CaO and MgO were identified as the new phases. CO_2 was determined to be the main volatile component by MS at temperatures between 1100 and 1145°C (Fig 8). Dolomite is a component of laterite [4]. Yoshida et al. investigated the decomposition of dolomite ores to CaO and MgO and found that CO_2 was released from the ores [30], which is consistent with our observations. However, our results partially contradict those reported by Conesa et al., who found that the primary decomposition temperature of dolomite was 780–800°C during the gasification and pyrolysis of *Posidonia oceanica* in the presence of dolomite [31]. Presumably, this difference was caused by the dispersion of dolomite in the laterite and the interaction with the laterite complex. The reaction [31] in the fourth stage of our study can be expressed by

$$Ca, Mg(CO_3)_2 \overset{1126^{\circ}C}{\rightarrow} CaCO_3 + MgCO_3 \quad (12)$$

$$Ca, Mg(CO_3)_2 \overset{1126^{\circ}C}{\rightarrow} CaO + MgO + 2CO_2 \quad (13)$$

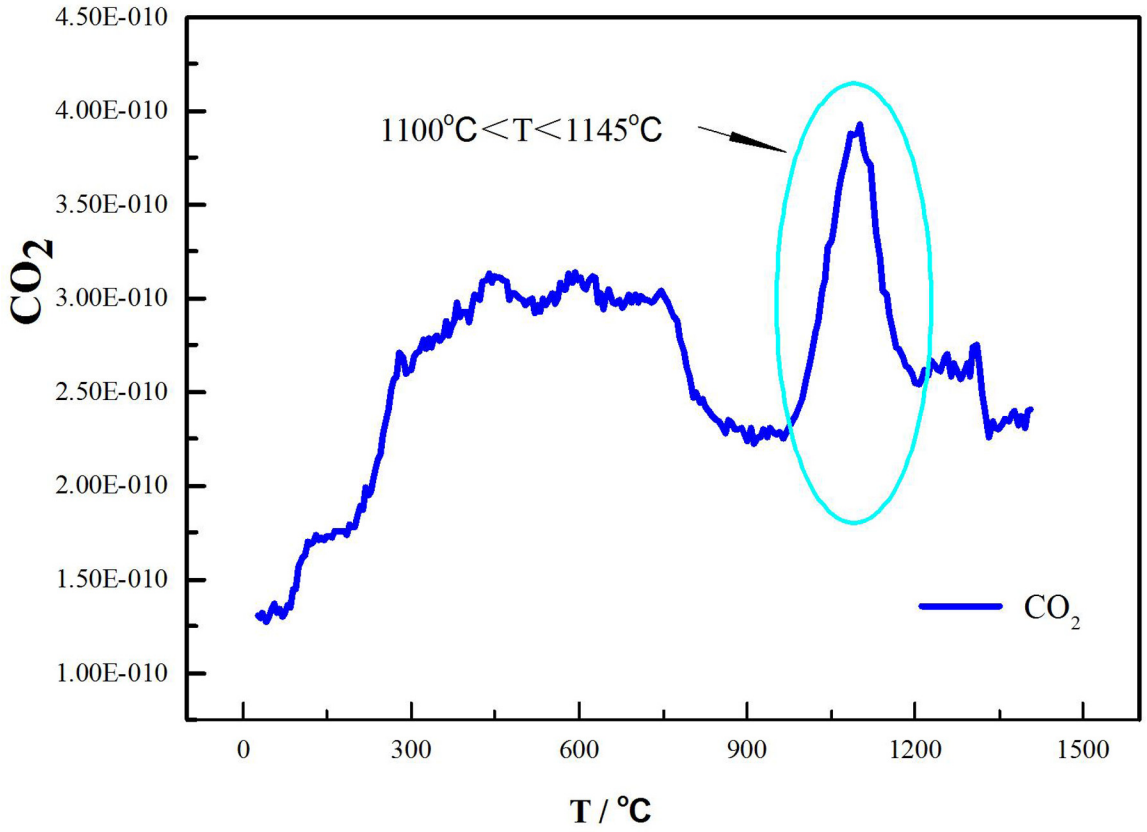

Fig 8. MS fragmentation intensities of CO_2 during the thermal decomposition of laterite.

doi:10.1371/journal.pone.0157369.g008

At temperatures between room temperature and 890°C, water was the product of laterite decomposition, which caused approximately 92% of the total mass loss. At temperatures above 890°C, the main volatile component was CO_2, which caused only 3% of the total mass loss.

Decomposition mechanism of the Na_2SO_4/laterite blends

To identify the mechanism of decomposition of the Na_2SO_4/laterite blends, the samples of the Na_2SO_4/laterite blend ores were roasted under a 100 ml/min Ar flow for 4 h at temperatures of 87°C, 268°C, 573°C, 897°C, and 1252°C.

Fig 9 shows the phase of the roasted ores, which were roasted under a 100 ml/min Ar flow for 4 h at temperatures of 84°C, 268°C, 573°C, and 897°C, as elucidated from the XRD patterns. The volatile component was analyzed by TG-MS. Fig 7 shows the variation in the H_2O content during the thermal decomposition of the Na_2SO_4/laterite blends.

Figs 2, 7 and 9 show that the decomposition of the Na_2SO_4/laterite blends can be divided into five stages. The decomposition ranges of the Na_2SO_4/laterite blends are similar to those of the laterite in the first three stages, and H_2O is the volatile component. Therefore, the first three stages are similar to the decomposition process of the laterite ores, which suggests that Na_2SO_4 does not affect laterite decomposition below 700°C. Increasing the roasting temperature to 892°C results in a sharp decrease in the amounts of the Na_2SO_4/laterite blends; a weight loss of approximately 14 wt% occurred between 897°C and 1300°C, where the laterite had experienced a weight loss of approximately 1 wt%. It can be inferred that Na_2SO_4 has a significant impact on the decomposition of laterite at temperatures above 897°C.

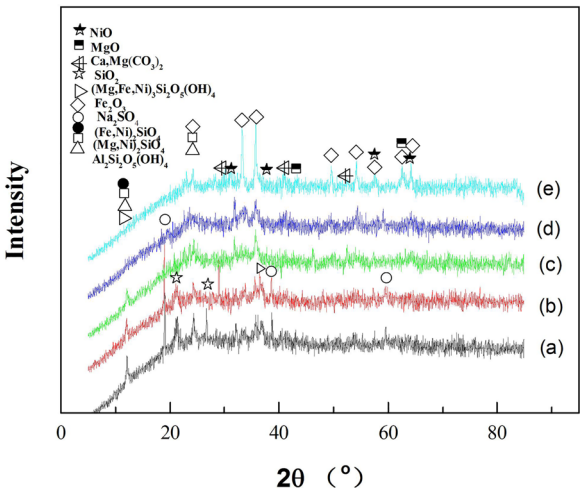

Fig 9. XRD patterns of the Na_2SO_4/laterite blends roasted under Ar at different temperatures. (a) raw ore, (b) 84°C, (c) 268°C, (d) 573°C, (e) 897°C.

doi:10.1371/journal.pone.0157369.g009

To determine whether the weight loss was caused by the Na_2SO_4 decomposition itself, pure Na_2SO_4 was heated under a 100 ml/min Ar flow from room temperature to 1300°C by TG-MS. Reagent-grade Na_2SO_4 was pyrogenated via thermogravimetric analysis, and no significant decomposition of Na_2SO_4 was observed. The result indicates that the mass loss of the Na_2SO_4/laterite blends cannot be due to Na_2SO_4 decomposition alone. Freyer et al. investigated the phase diagram of the Na_2SO_4—$CaSO_4$ system and found that Na_2SO_4 cannot be decomposed until 1404°C [32], which indicates that the mass loss of Na_2SO_4/laterite blends cannot be caused by only Na_2SO_4 decomposition. In addition, SO_2 was detected by MS (Fig 10) along with the emitted CO_2 beginning at 892°C. Based on the MS fragmentation intensities of CO_2 during the thermal decomposition of the Na_2SO_4/laterite blends (Fig 11), the initial temperature of CO_2 emission is 897°C, which is 200°C lower than the decomposition temperature of the laterite.

The roasted products of the Na_2SO_4/laterite blends, which were roasted at 897°C for 4 h, were detected by XRD. CaO and MgO were found in the roasted residue (Fig 9). Gunasekaran et al. investigated the thermal decomposition of natural dolomite and found that the decomposition temperature of dolomite is 600–850°C [33], which indicates that in the presence of Na_2SO_4, the decomposition temperature of dolomite can be reduced to nearly the decomposition temperature of natural dolomite. Lu et al. investigated the reduction of prepared nickel laterite ore by H_2. The experiments were conducted at 800°C with the addition of 20 wt% Na_2SO_4 and obtained a maximum nickel content of 5.63% and a nickel recovery of 83.59% [9], which indicates that the pyrometallurgical operating temperature can be reduced to a range of 892–1080°C in the presence of Na_2SO_4, which is approximately 200°C lower than in the conventional process [7]. Therefore, in the fourth stage (897°C<T<914°C), it can be inferred that dolomite can be decomposed in the presence of the Na_2SO_4 in this temperature range. The process is described in the literature [9,32] and can be expressed as Eq (12) and Eq (13).

Nevertheless, it is worth investigating whether the CaO, which decomposed from the dolomite, can affect the emission of SO_2, as the CaO can react with SO_2 to form $CaSO_3$. Cubicciotti et al. investigated the thermal decomposition of $CaSO_3$ and its enthalpy of formation and found that $CaSO_3$ decomposed in the temperature range of 500–550°C [34]. Therefore, $CaSO_3$ could not stably exist between 897°C and 914°C. In addition, the content of dolomite in the

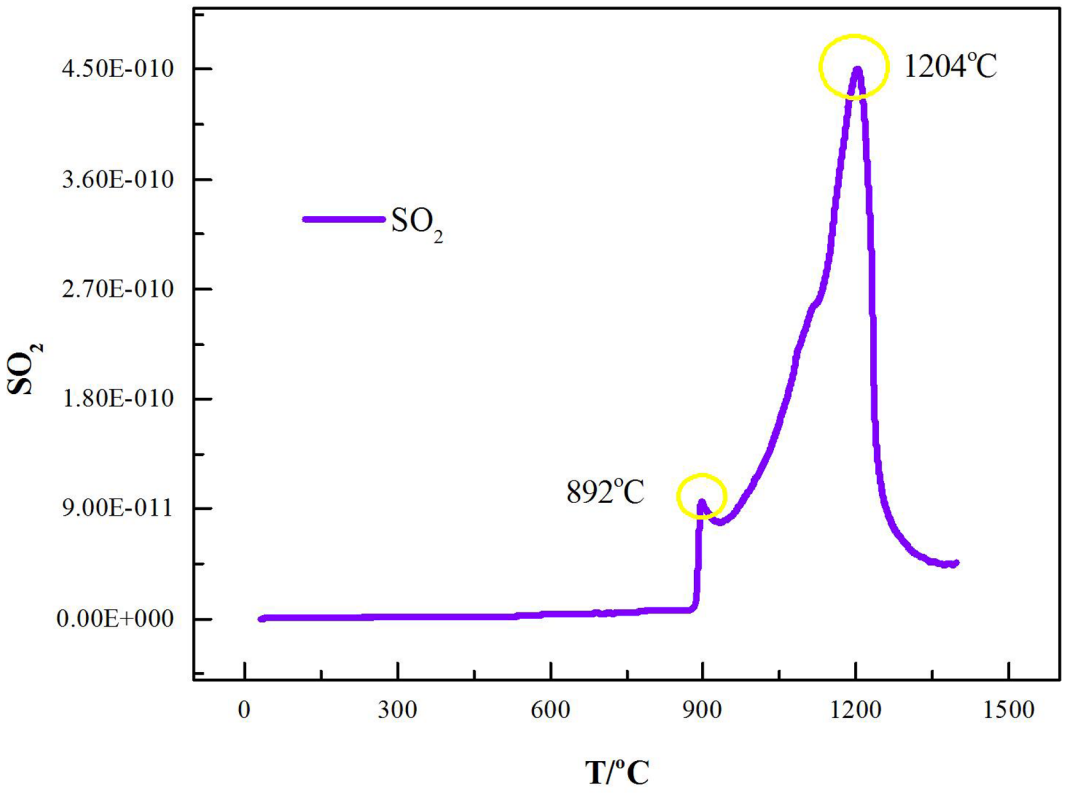

Fig 10. MS fragmentation intensities of SO_2 during thermal decomposition of the Na_2SO_4/laterite blends.

doi:10.1371/journal.pone.0157369.g010

laterite ores was low and the amount of CaO released would be low. Therefore, the presence of CaO would have little influence on the emission of CO_2 and SO_2.

In the last stage (1241°C<T<1286°C), CO_2 and SO_2 were the main volatiles of the decomposition of the Na_2SO_4/laterite blends (Fig 10). Based on the products of the fourth stage of the decomposition of the Na_2SO_4/laterite blends, CO_2 may be generated by the decomposition of the dolomite. Lu et al. investigated the standard Gibbs free energy and temperature diagram and found that SO_2 was released from the ores at temperatures above 727°C [9]. Our results show that Na_2SO_4 reacted with laterite and emitted SO_2, which was consistent with results that have been reported in the literature [9].

To determine what occurs when Na_2SO_4 reacts with laterite, the decomposition products, which were roasted at 1252°C for 4 h, were analyzed by XRD (Fig 12). $(Mg,Ni)_2SiO_4$, $(Mg,Ni)_2SiO_4$, $(Fe,Ni)_2SiO_4$ and $(Fe,Ni)_2SiO_4$ disappeared (Fig 9D), and several new phases formed, such as $(Mg,Na)_2SiO_4$, Na_2SiO_3, $(Mg,Na)_2SiO_4$ and Na_2SiO_3. Li et al. investigated the purification of nickeliferous laterite by reduction roasting in the presence of sodium sulfate and found that sodium sulfate can liberate Fe and Ni from lizardite and leave behind an Mg-rich olivine phase [12]. The results of this study show that the main residue of the Na_2SO_4/laterite blends under 1252°C in the last stage were consistent with those that have been reported in the literature [12]. Therefore, Na_2SO_4 reacted with $(Mg,Ni)_2SiO_4$ and $(Mg,Ni)_2SiO_4$, and a considerable amount of Na^+ then replaced Ni^{2+} in $(Mg,Ni)_2SiO_4$ and $(Mg,Ni)_2SiO_4$. Meanwhile, the free Ni^{2+} formed NiO, which is beneficial for the ensuing nickel enrichment.

Mobin et al. found that transition-metal carbides interact with Na_2SO_4 to form a soluble sodium metal oxide or a metal sulfide depending upon the local conditions during the high

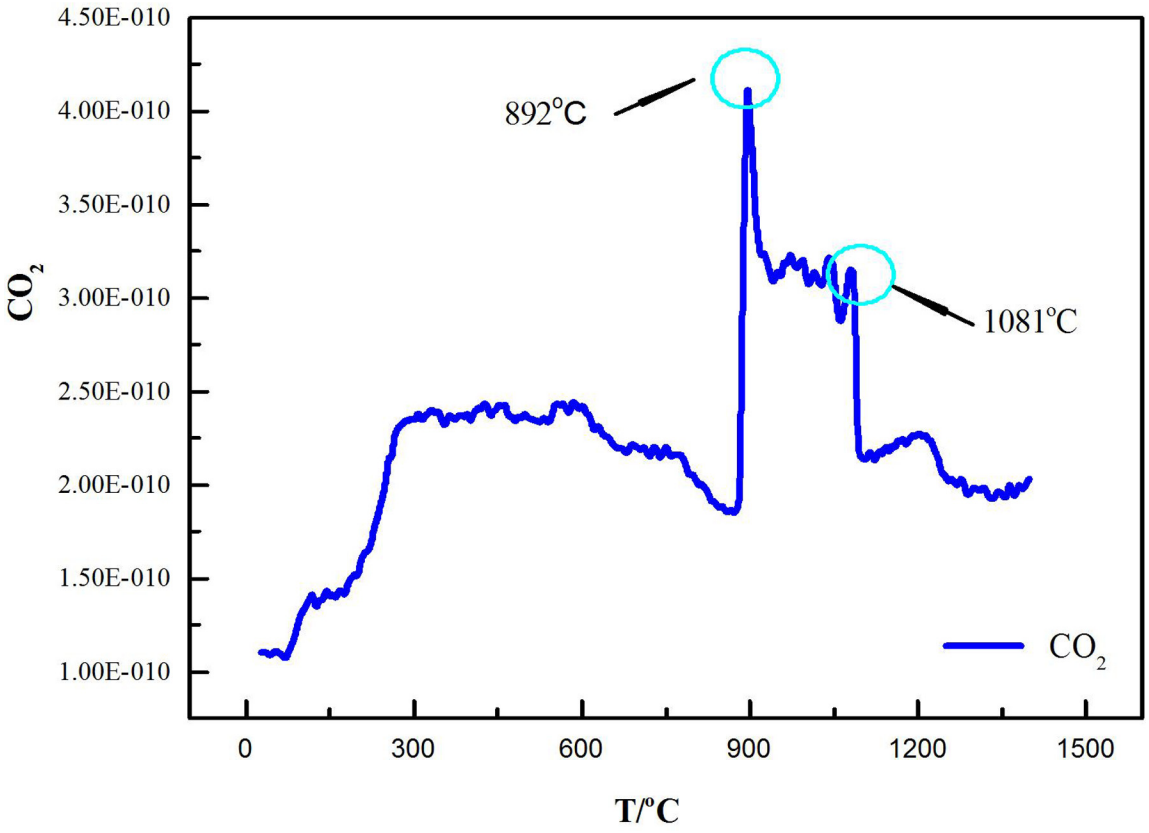

Fig 11. MS fragmentation intensities of CO_2 during thermal decomposition of the Na_2SO_4/laterite blends.

doi:10.1371/journal.pone.0157369.g011

temperature reaction [35]. Our research shows that the Na_2SO_4/laterite blends reach the molten state after roasting at 1252°C for 4 h, which is consistent with results from the literature [12].

Alkali ions preferentially take up next-nearest neighbor positions with respect to tetrahedral Fe^{3+} ions [36]. In our study, the Na^+ replaced Fe^{3+} and Mg^{2+} in $(Mg,Ni)_2SiO_4$ and $(Mg,Ni)_2SiO_4$ to form Na_2SiO_3. Composite materials with mixed spinel nickel ferrite–barium titanate as co-existing phases can be synthesized [37]. Therefore, the Fe_2O_3, NiO and MgO that are released from $(Mg,Ni)_2SiO_4$ and $(Mg,Ni)_2SiO_4$ then react and form $MgFe_2O_4$ and $NiFe_2O_4$ (Eqs 14, 19 and 20). At the same time, Na^+ replaces some of the Al^{3+} in the $Al_2Si_2O_7$ and forms $NaAlSiO_4$ (Eq 17). O'Neill et al. experimentally investigated the effect of the melt composition on trace element partitioning based on the activity coefficients of FeO, NiO, CoO, MoO_2 and MoO_3 in silicate melts and found that the activity coefficients of FeO, NiO and CoO vary by a factor of two over the same range of melt compositions [38]. In this study, we found that all of the materials combine to form a hard low-melting-point amorphous substance at high temperature with some alkaline metals. In the last stage of the laterite with and without the addition of Na_2SO_4, this mechanism is supported by the phase composition of the decomposition products (Fig 12) and the MS fragmentation intensities of SO_2 during the decomposition at temperatures between 1241 and 1286°C (Fig 10). Therefore, the mechanism of laterite decomposition by Na_2SO_4 involved reacting some of the Na_2SO_4 with the calcined laterite ores, which resulted in laterite decomposition and the release of Ni^{2+} from the laterite and is beneficial for nickel

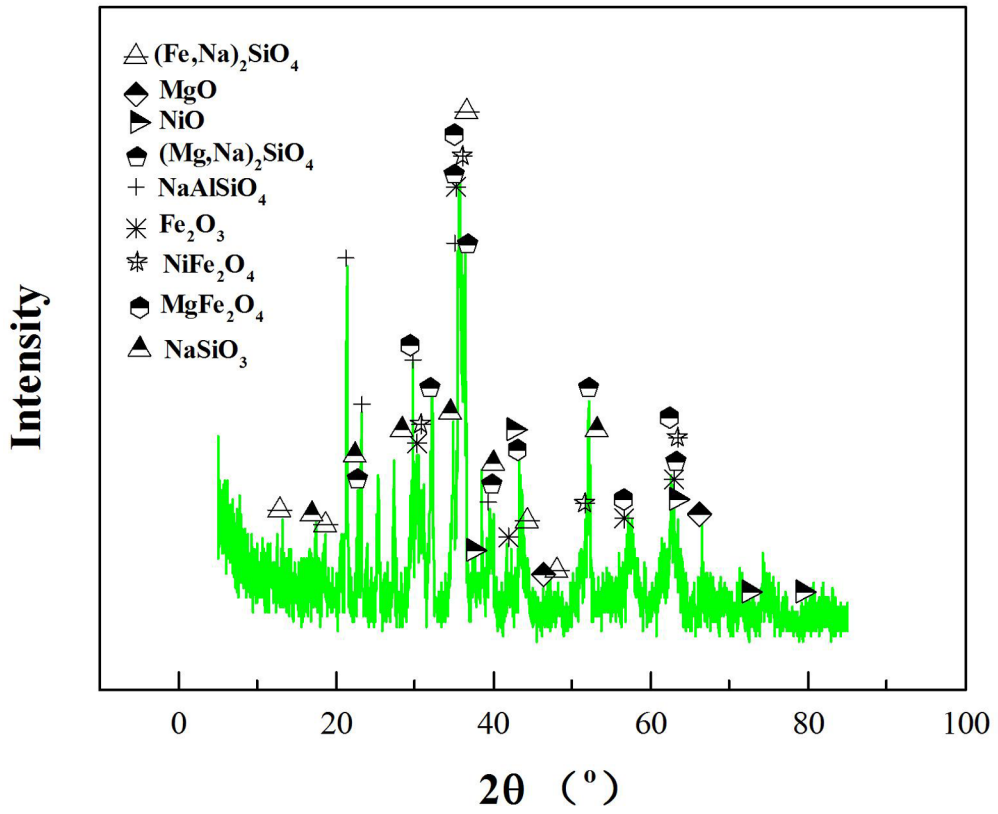

Fig 12. XRD patterns of the Na_2SO_4/laterite blends roasted under Ar at 1252°C for 4 h.

doi:10.1371/journal.pone.0157369.g012

enrichment. This process can be expressed as follows:

$$(Mg, Ni)_2SiO_4 + Na_2SO_4 = (Mg, Na)_2SiO_4 + 2NiO + SO_2(g) \quad (14)$$

$$(Mg, Ni)_2SiO_3 + Na_2SO_4 = Na_2SiO_3 + 2MgO + 2NiO + SO_2(g) \quad (15)$$

$$(Fe, Ni)_2SiO_4 + Na_2SO_4 = (Fe, Na)_2SiO_4 + 2NiO + SO_2(g) \quad (16)$$

$$(Fe, Ni)_2SiO_3 + Na_2SO_4 = Na_2SiO_3 + 2Fe_2O_3 + 2NiO + SO_2(g) \quad (17)$$

$$Al_2Si_2O_7 + Na_2SO_4 = 2NaAlSiO_4 + SO_2(g) \quad (18)$$

$$Fe_2O_3 + MgO = MgFe_2O_4 \quad (19)$$

$$Fe_2O_3 + NiO = NiFe_2O_4 \quad (20)$$

Reduction results

Reduction roasting-magnetic separation of the laterite with/without Na_2SO_4. In the absence of Na_2SO_4, hydrogen reduction roasting-magnetic separation was conducted at 700, 800 and 900°C. The other experimental conditions were fixed, including the reducing time of 120 min, the gas rate of 2.7 L/min (H_2:70%, N_2:30%), grinding fineness of 90 wt% passing 0.043 mm and magnetic field intensity of 0.1 T. Fig 13 shows that the grade and recovery of Ni

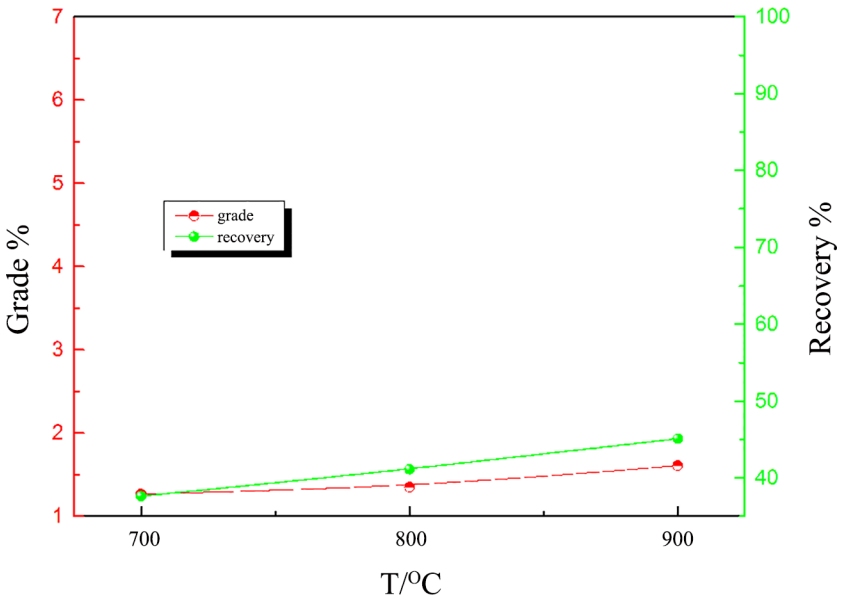

Fig 13. The effect of the reduction temperature on nickel–iron beneficiation (reduced for 120 min).

doi:10.1371/journal.pone.0157369.g013

increases with increasing roasting temperature from 700 to 900°C. However, only a maximum of 1.61% Ni grade with recovery of 45.09% Ni is achieved at 900°C.

When the nickel laterite ore with the addition of 20 wt% Na_2SO_4 was reduced at 700, 800 and 900°C for 120 min, the Ni grade increased from 2.06% to 6.01% and the recovery of Ni increased from 58.29% to 100% from 700°C to 900°C, as shown in Fig 14. The roasting reduction temperature of the commercially existing pyrometallurgical process for nickel from nickel

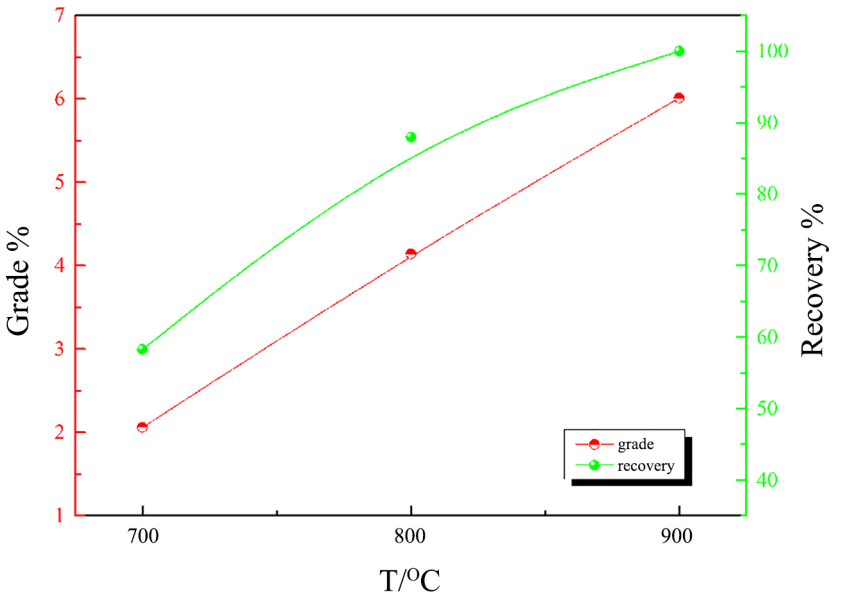

Fig 14. The effect of the reduction temperature on nickel–iron beneficiation (reduced for 120 min in the presence of 20 wt% sodium sulphate).

doi:10.1371/journal.pone.0157369.g014

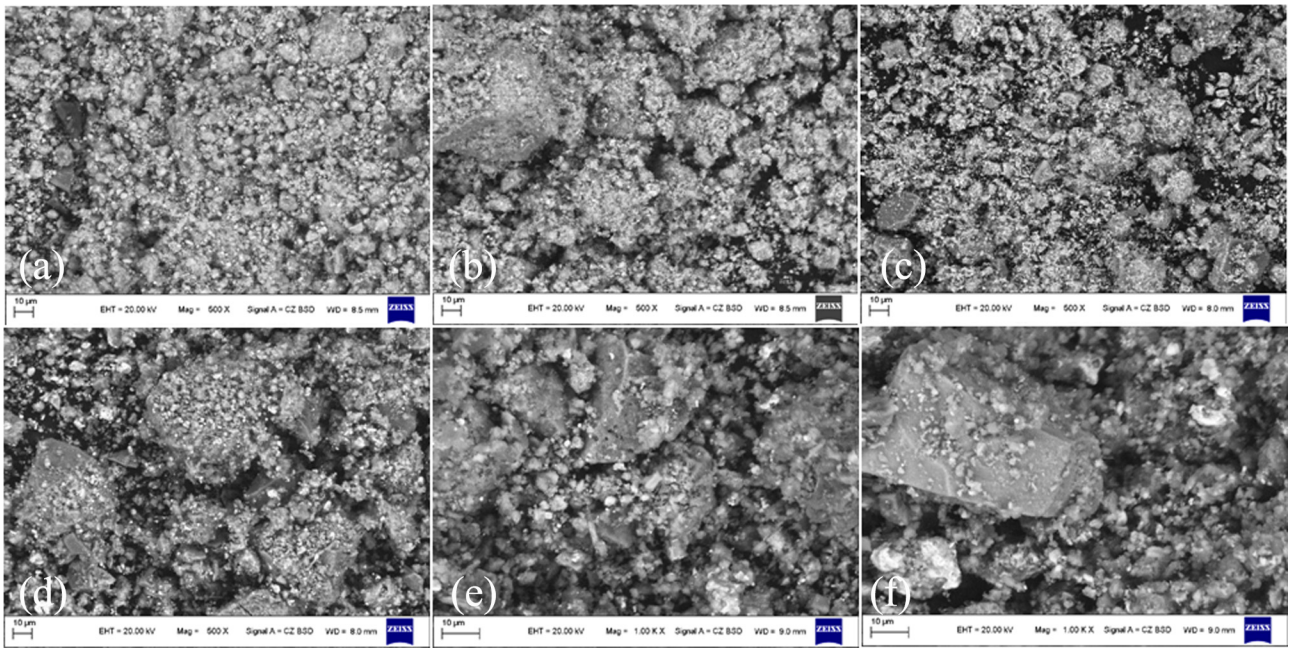

Fig 15. SEM images (backscattered electron images) of the roasted ores. (a)-(c) General overview of microstructure of mineral particles and the roasted ores without Na_2SO_4 at 700°C, 800°C, and 900°C, respectively. (d)-(f) General overview of microstructure of mineral particles and the roasted ores with 20 wt% Na_2SO_4 at 700°C, 800°C, and 900°C, respectively.

doi:10.1371/journal.pone.0157369.g015

laterite is 1250–1400°C [12]. Therefore, in terms of operating temperature, the reduction in operating temperature to 900°C in the current work is an advantage.

SEM analysis. To reveal the effects of the Na_2SO_4 on the beneficiation of laterite ore, the reduced products were analyzed by SEM. The microstructure of the roasted ore (with/without Na_2SO_4) at different temperatures are shown in Fig 15.

Fig 15(A)–15(C) show the general microstructure of the roasted ores of laterite. The structure of the roasted ore is loose with a dispersed metallic mineral distribution. Furthermore, the roasted ore of Na_2SO_4/laterite blends exhibits a saponaceous surface and a compact structure as shown in Fig 15D–15F, which indicates that the roasted ore is molten with Na_2SO_4 during the reduction process [13]. The molten phase is beneficiated to achieve rapid grain coarsening and a higher concentration of Ni [9–12].

Conclusions

The results of this study can be summarized as follows:

1. The decomposition of laterite can be divided into four stages: water evaporation, goethite decomposition, kaolinite and serpentine dehydroxylation, and dolomite decomposition with CO_2 as the main volatile component. The activation energies for the different stages were 45.64 kJ/mol, 87.13 kJ/mol, 123.63 kJ/mol and 145.66 kJ/mol, respectively.
2. The decomposition of Na_2SO_4/laterite blends can be divided into five stages. The decomposition process is similar to that of laterite blends at 700°C. However, dolomite decomposed at 200°C lower than the temperature at which laterite decomposed in the fourth stage, and the activation energy was 108.50 kJ/mol. In the final stage, laterite decomposed in the presence of Na_2SO_4 and emitted SO_2 with an activation energy of 91.37 kJ/mol.

3. Kinetic analyses revealed that the decomposition of laterite with and without the addition of Na_2SO_4 in an argon atmosphere can be described by one first-order reaction, However, Na_2SO_4 significantly influences laterite decomposition through direct involvement and can reduce the activation energy of laterite decomposition; thus, the reaction rate can be accelerated, and the reaction temperature can be markedly reduced.

4. The mechanism of the decomposition of Na_2SO_4/laterite blends may involve the reaction of Na_2SO_4 with laterite and the consequent decrease in the laterite decomposition temperature. Na^+ was then replaced with Ni^{2+}, which is an isomorphic host in the lattice of $(Ni, Mg)_2SiO_4$. Ni^{2+} was released and reacted with O^{2-} to form NiO, which facilitated nickel enrichment through the ensuing reduction. At the same time, Na_2SO_4 reacted with Mg_2SiO_4 and Fe_2SiO_4 to form low-melting-point compounds.

5. The roasted ore with the addition of Na_2SO_4 exhibits a compact structure and can be formed in the molten phase with Na_2SO_4 during the reduction process. The molten phase is beneficiated to achieve rapid grain coarsening and a higher concentration of Ni. Moreover, the pyrometallurgical operating temperature can be reduced to a range of 892–1080°C in the presence of Na_2SO_4, which is approximately 200°C lower than in the conventional process.

Acknowledgments

This work was financially supported by the National Natural Science Foundation of China (No. 21276172) and was sponsored by the Taiyuan Green Coke Clean Energy Co., Ltd. (China).

Author Contributions

Conceived and designed the experiments: SY WGD. Performed the experiments: PZS. Analyzed the data: SJL CHZ. Contributed reagents/materials/analysis tools: PC QZ HLF. Wrote the paper: SY JSG.

References

1. Reck BK, Müller DB, Rostkowski K, Graedel TE. Anthropogenic nickel cycle: Insights into use, trade, and recycling. Environ Sci Technol. 2008; 42: 3394–3400. PMID: 18522124
2. Hidayat T, Rhamdhani MA, Jak E, Hayes PC. The characterization of nickel metal pore structures and the measurement of intrinsic reaction rate during the reduction of nickel oxide in H2–N2 and H2–H2O atmospheres. Miner Eng. 2008; 21: 157–166.
3. Quast K, Connor JN, Skinner W, Robinson DJ, Addai-Mensah J. Preconcentration strategies in the processing of nickel laterite ores Part 1: Literature review. Miner Eng. 2015a; 79: 261–268.
4. Katzagiannakis N, Alevizos G, Stamboliadis E, Stratakis A, Petrakis E. Mineralogical Investigation and Washability Treatment of the Nickeliferous Lateritic Deposit of Nome (Albania). Geomaterials 2014; 4: 105–115.
5. Khataee A, Salahpour F, Fathinia M, Seyyedi B, Vahid B. Iron rich laterite soil with mesoporous structure for heterogeneous Fenton-like degradation of an azo dye under visible light. J Ind Eng Chem. 2015; 26: 129–135.
6. Zhu D, Cui Y, Hapugoda S, Vining K, Pan J. Mineralogy and crystal chemistry of a low grade nickel laterite ore. Transactions of Nonferrous Metals Society of China 2012; 22: 907–916.
7. Li B, Wang H, Wei Y. The reduction of nickel from low-grade nickel laterite ore using a solid-state deoxidisation method. Miner Eng. 2011; 24: 1556–1562.
8. Norgate T, Jahanshahi S. Assessing the energy and greenhouse gas footprints of nickel laterite processing. Miner Eng. 2011; 24: 698–707.
9. Lu J, Liu S, Shangguan J, Du W, Pan F, Yang S. The effect of sodium sulphate on the hydrogen reduction process of nickel laterite ore. Miner Eng. 2013; 49: 154–164.

10. Quast K, Connor JN, Skinner W, Robinson DJ, Li J, Addai-Mensah J. Preconcentration strategies in the processing of nickel laterite ores part 2: Laboratory experiments. Miner Eng. 2015b; 79: 269–278.
11. Jiang M, Sun T, Liu Z, Kou J, Liu N, Zhang S. Mechanism of sodium sulfate in promoting selective reduction of nickel laterite ore during reduction roasting process. Int J Miner Process. 2013; 123: 32–38.
12. Li G, Shi T, Rao M, Jiang T, Zhang Y. Beneficiation of nickeliferous laterite by reduction roasting in the presence of sodium sulfate. Miner Eng. 2012; 32: 19–26.
13. Jiang M, Sun T, Liu Z, Kou J, Liu N, Zhang SY. Mechanism of sodium sulfate in promoting selective reduction of nickel laterite ore during reduction roasting process. Int J Miner Process. 2013; 123: 32–38.
14. Katzagiannakis N, Alevizos G, Stamboliadis E, Stratakis A, Petrakis E. Mineralogical investigation and washability treatment of the nickeliferous lateritic deposit of nome (Albania). Geomaterials 2014; 4: 105–115.
15. Anandakumaran P, Bhattacharya A. TG-DTA studies on the pyrolysis of limestone—laterite mixtures. Thermochim Acta. 1982; 59: 319–329.
16. Cai J, Zhang L, Zhang F, Wang Z, Cheng Z, Yuan W, et al. Experimental and Kinetic Modeling Study of n-Butanol Pyrolysis and Combustion. Energ Fuel. 2012; 26: 5550–5568.
17. Mitchell SL. Applying the combined integral method to two-phase Stefan problems with delayed onset of phase change. J Comput Appl Math. 2015; 281: 58–73.
18. Zhang Q, Li Q, Zhang L, Wang Z, Jing X, Yu Z, et al. Preliminary study on co-gasification behavior of deoiled asphalt with coal and biomass. Appl Energ. 2014; 132: 426–434.
19. Vyazovkin S, Wight CA. Isothermal and non-isothermal kinetics of thermally stimulated reactions of solids. Int Rev Phys Chem. 1998; 17: 407–433.
20. Ghaffari M, Ehsani M, Khonakdar HA, Assche GV, Terryn H. The kinetic analysis of isothermal curing reaction of an epoxy resin-glassflake nanocomposite. Thermochim. Acta. 2012; 549: 81–86.
21. Liu W, Wang Q, Zhang J, Xie XH, Liu HH, Min GQ, et al. Isothermal kinetic analysis of the effects of high-energy ball milling on solid-state reaction of $Li_4Ti_5O_{12}$. Powder Technol. 2016; 287: 373–379.
22. Mabuda AI, Mamphweli NS, Meyer EL. Model free kinetic analysis of biomass/sorbent blends for gasification purposes. Renew Sust Energ Rev. 2016; 53: 1656–1664.
23. Ozawa T. Kinetic analysis of derivative curves in thermal analysis. J Therm Anal Calorim. 1970; 2: 301–324.
24. Cai J, Wang Y, Zhou L, Huang Q. Thermogravimetric analysis and kinetics of coal/plastic blends during co-pyrolysis in nitrogen atmosphere. Fuel Process Technol. 2008; 89: 21–27.
25. Jaber JO, Probert SD. Pyrolysis and gasification kinetics of Jordanian oil-shales. Appl Energ. 1999; 63: 269–286.
26. Jacobson NS. Sodium sulfate: deposition and dissolution of silica. Oxid Met. 1989; 31: 91–103.
27. Kaupp G, Naimi-Jamal M R, Schmeyers J. Solvent-free Knoevenagel condensations and Michael additions in the solid state and in the melt with quantitative yield. Tetrahedron. 2003; 59: 3753–3760.
28. Jang K, Nunna VRM, Hapugoda S, Nguyen AV, Bruckard WJ. Chemical and mineral transformation of a low grade goethite ore by dehydroxylation, reduction roasting and magnetic separation. Miner Eng. 2014; 60:14–22.
29. Park JO, Kim HS, Jung SM. Use of oxidation roasting to control NiO reduction in Ni-bearing limonitic laterite. Miner Eng. 2015; 71: 205–215.
30. Yoshida M, Koilraj P, Qiu X, Hirajima T, Sasaki K. Sorption of arsenate on MgAl and MgFe layered double hydroxides derived from calcined dolomite. J Environ Chem Eng. 2015; 3: 1614–1621.
31. Conesa JA, Domene A. Gasification and pyrolysis of Posidonia oceanica in the presence of dolomite. J Anal Appl Pyrol. 2015; 113, 680–689.
32. Freyer D, Voigt W, Köhnke K. The phase diagram of the system Na2SO4—CaSO4. European Journal of Solid State and Inorganic Chemistry 1998; 35: 595–606.
33. Gunasekaran S, Anbalagan G. Thermal decomposition of natural dolomite. B Mater Sci. 2007; 30: 339–344.
34. Cubicciotti D, Sanjurjo A, Hildenbrand DL. The thermal decomposition of $CaSO_3$ and its enthalpy of formation. J Electrochem Soc. 1977; 124: 933–936.
35. Mobin M, Malik AU. High-temperature interactions of transition-metal carbides with Na2SO4. Journal of the Less Common Metals 1991; 170: 243–254.

36. Bingham PA, Parker JM, Searle TM, Smith I. Local structure and medium range ordering of tetrahedrally coordinated Fe3+ ions in alkali–alkaline earth–silica glasses. J non-cryst solids. 2007; 353: 2479–2494.

37. Francis A, Daoush W. Synthesis and magnetic characteristics of crystallized ceramic in the BaO–NiO–TiO2–Fe2O3 system. J Mater Process Technol. 2007; 181: 213–216.

38. O'Neill HSC, Eggins SM. The effect of melt composition on trace element partitioning: an experimental investigation of the activity coefficients of FeO, NiO, CoO, MoO2 and MoO3 in silicate melts. Chem Geol. 2002; 186: 151–181.